REVIEW

Journal of Optics and Photonics Research 2025, Vol. 00(00) 1–12

DOI: 10.47852/bonviewJOPR52025894



Optical Antireflective Layered and Nanoporous Metamaterials for Optoelectronic Devices

Nickolay M. Ushakov^{1,2,*}, I. D. Kosobudskiy¹ and M. Yu. Vasilkov^{1,2}

¹Saratov Branch, V.A. Kotelnikov Institute of Radio Engineering and Electronics of the Russian Academy of Sciences, Russia

Abstract: This paper presents an overview of new ideas for creating antireflective coatings for protective glasses of optoelectronic devices based on layered and matrix metamaterials with extended functionality. Attention is drawn to such important types of metamaterials as layered porous and polymer composite nanomaterials. For layered antireflective nanostructures, distinctive optical properties of coatings achieved by controlling the composition and thickness of the layers are highlighted. Composites of silicon and titanium dioxide are considered the main materials of multilayer coatings. For single-layer coatings, attention is paid to polymer matrix composite nanomaterials based on polymethyl methacrylate with the inclusion of silver nanoparticles. Metaglasses (glass plates with a two-layer deposition of silver films) or membranes made of porous anodic aluminum oxide with a thin gold film are proposed to be used as electrically conductive transparent optical elements. The article discusses the technology of creating antireflective coatings and their optical properties. At the same time, among many known technological methods for creating antireflective coatings on glass substrates, special attention is paid to sol-gel technology as technically simple and having wide functional capabilities. The optical properties of the coatings were assessed by their spectral-optical characteristics of reflection and transmission in the range of 300–1000 nm.

Keywords: antireflective coatings, metamaterials, nanocomposites, porous oxides

1. Introduction

For most devices of various purposes in the optical and subwavelength (terahertz) range, solving problems related to reducing losses due to reflection of incident electromagnetic radiation (EMR) remains relevant. For this purpose, antireflection coatings (ARCs) are developed, which are applied either to protective dielectric substrates or directly to active semiconductor substrates [1, 2]. At the same time, in order to minimize the reflection of EMR from the interface between the coating and air, it is necessary to provide the most complete broadband optical matching by impedance of the substrate with the coating and the environment. It is known that the impedance of the medium is determined by the inverse value of the modulus of its complex refractive index, as $Z_m = \frac{Z_0}{\sqrt{n^2 + k^2}}$, where $Z_0 = 377\text{Ohm}$, n is the refractive index, and k is the absorption coefficient or extinction coefficient. In essence, the ARC is a transformer of the impedances of the environment and the substrate. For transparent and absorbing substrates, ARCs should provide optical transparency to light. Ideal enlightenment occurs when the condition $Z_m = Z_0$ or $\sqrt{n^2 + k^2} = 1$ is met.

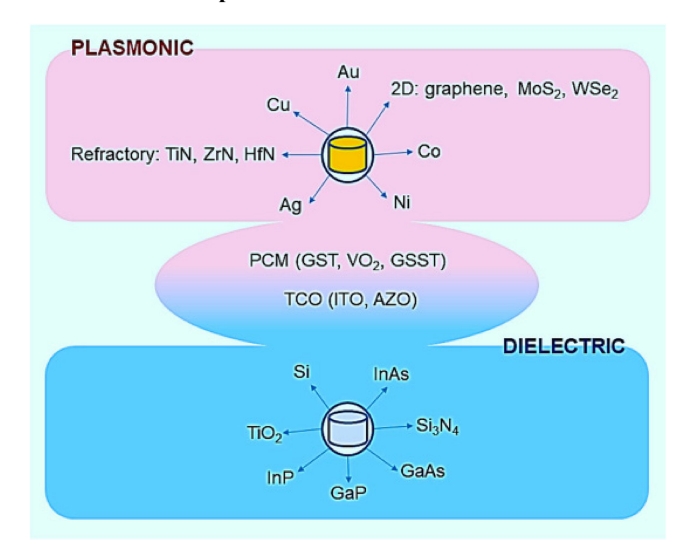
The ARCs themselves can be made of multilayer oxide (ZnO/TiO₂; SiO₂/TiO₂) [3, 4] or single-layer polymer (Ag@PMMA) composite nanomaterials [5]. The creation and use of ARCs based on layered optically transparent media is now the most promising way to match a device with its environment using broadband optical technology, such as mesoporous [6] and hyperbolic metamaterials [7]. Such metamaterials are capable of significantly reducing light reflection in a wide range of wavelengths [8].

Metamaterials and metasurfaces (2D metamaterials) play an important role in expanding the functionality of materials [9]. Typically, subwavelength metal structures are used as the basis for the structure of metasurfaces. However, metal structures have ohmic losses, especially in the optical range, which limits the functionality of devices with such materials. As an alternative to materials with subwavelength metal structures, dielectric materials with low losses and a high refractive index have received attention in recent years. Such metasurfaces are 2D arrays of dielectric resonators. By tuning magnetic and electric resonances by adjusting the geometric dimensions and distance between dielectric resonators, it is possible to expand the functionality of metasurfaces without using metal structures. In general, metasurfaces fall into one of two categories: dielectric or electrically conductive (plasmonic). Other materials, such as transparent conducting oxides (TCOs) and phase-change materials, can reversibly change from plasmonic to dielectric characteristics when exposed to external influences. External action

²Saratov National Research State University named after N.G. Chernyshevsky, Russia

^{*}Corresponding author: Nickolay M. Ushakov, Saratov Branch, V.A. Kotelnikov Institute of Radio Engineering and Electronics of the Russian Academy of Sciences, Russia. Email: nmu@bk.ru

Figure 1
Materials of plasmonic and dielectric metasurfaces



provides a phase change (from a crystalline state to an amorphous one or vice versa) or by moving charge carriers into the conduction zone.

Figure 1 [9] shows a structural diagram of materials for metasurfaces of two main classes: plasmonic and dielectric.

To increase the radiation efficiency and compactness of the devices, dielectric resonators are mounted on a metal ground plane. Two-dimensional structures of spherical silicon nanoparticles represent a unique optical system. These low-loss dielectric nanoparticles have high magnetic resonance properties (Mie resonances). As a result, strong electrical and magnetic optical scattering occurs, which depends on the size and structure of the dielectric particles [10-14]. The basic mechanism for excitation of such modes inside the nanoparticles is similar to the excitation mechanism of split-edge ring resonators. However, there is one important difference: silicon nanoparticles have much lower losses and are able to shift the magnetic resonance wavelength to the visible range. Optical systems made of dielectric two-dimensional low-loss metamaterials open up new prospects for creating nanophotonic devices. Materials in the shape of silicon nanospheres or nanodisks show promise for the creation of dielectric twodimensional metamaterials in the optical wavelength range. For example, in Adachi et al. [14], a nanoprobe based on a silicon nanosphere with a diameter of 100-200 nm was proposed, providing visualization of Mie scattering independent of the environment.

Recently, near-zero epsilon (ENZ) metamaterials have attracted attention due to their anomalous electromagnetic properties over a wide wavelength range [15–19]. In ENZ metamaterials, the permittivity tends to zero at frequencies close to the plasma frequency. When working with ENZ metamaterials in the visible or near-infrared (IR) portion of the optical spectrum, nanocomposites based on the incorporation of noble metal nanoparticles in a dielectric matrix show promise. Nanocomposites based on the integration of noble metal nanoparticles in a dielectric matrix exhibit potential when working with ENZ metamaterials in the visible or near-IR region of the optical spectrum. A rapidly growing research area that has attracted great scientific interest is the development and characterization of metasurfaces for ARCs [20, 21].

In this review, the main objective is to provide new ideas for designing layered and matrix metamaterial-based coatings with advanced functionalities. We collect published structural solutions and highlight the distinctive optical properties of the coatings achievable by controlling the composition and phase thicknesses. We expect this review to provide new insights for researchers in the field of optical material science. In this regard, we draw attention to such important types of metamaterials as composite and porous nanomaterials.

2. Porous and Polymer Composite Nanomaterials

In recent years, many studies have been devoted to the development of technological methods and the study of new porous metamaterials. In particular, porous materials such as porous silicon (pSi), silicon dioxide (SiO₂), porous anodic alumina, and titanium dioxide nanotube arrays (TiNT) are the best choice as antireflective coatings for photovoltaic (PV) and sensor devices [22–24].

To create composites based on porous ceramic membranes, the method of electrochemical deposition of metal and dielectric nanostructures into the pores of the membranes is used. The electrochemical process requires less expensive equipment than other metal deposition techniques like chemical vapor deposition or thermal deposition of metals. In works by Eessaa and El-Shamy [25] and Shang et al. [26], using the electrochemical method, metal nanostructures grown in the pores of the membrane of anodic aluminum oxide (nanowires, nanorods, nanotubes, and nanoparticles) were obtained. An important point is the formation of complex nanostructures by synthesizing various porous metals using electrochemical anodization.

Along with electrochemical deposition, a hybrid sol-gel method for synthesizing nanostructures has recently proven to be a promising method for creating composite nanomaterials based on porous anodic aluminum oxide (PAAO). Silicon and metal oxides (such as TiO₂, TiO₂/Si–silica composite, SnO₂, NiO, etc.) are the most often used materials for sol-gel synthesis of nanostructures utilizing PAAO matrices. This technique works by hydrolyzing the precursor sol on the PAAO support using the dip-coating approach and then allowing the solvent to evaporate and a glassy gel to develop inside the pores. A further heat treatment eliminates the remaining solvent from the gel-PAAO system. High-purity homogeneous and multicomponent structures can be synthesized using the sol-gel approach, which also allows for additional control over their structure, thermal stability, and surface reactivity [27–29].

Light interacts with noble metal nanoparticles to produce plasmonic oscillations of a specific frequency that are concentrated around the nanoparticles. Consequently, plasmonic materials exhibit surface plasmon resonance (SPR) and its variants, including waveguide and localized surface plasmon resonance (LSPR or LPR). SPR oscillations depend on the medium surrounding the nanoparticles, as well as on the size and shape of the nanoparticles themselves. SPR is sensitive to changes in the local refractive index of the medium. These changes can be measured using shifts in the resonance frequency [30, 31].

Optical modeling, fabrication, and characterization measurements for a broadband ARC on a silicon substrate based on Ag/mcSi nanocomposite are described in Walshe et al. [32]. ARCs (Ag/MMA) based on Ag nanoparticles embedded in a polymethyl methacrylate (PMMA) matrix for PV devices were modeled. A 52% increase in photocurrent was predicted compared to a conventional PV device. The modeling results showed that reducing the coating layer thickness further increased the total electrical power generation of the PV cell by 55% even in the absence of plasmonic photoluminescence.

2.1. Technology

Porous silica coatings produced through sol-gel technology possess a low refractive index, along with outstanding abrasion resistance and durability. Conversely, coatings based on titanium dioxide feature high transmittance and a high refractive index. The combination of such materials allows flexible control of the optical refractive index and the creation of effective broadband and durable antireflective coatings [33–35].

The sol-gel technology for the synthesis of composite coating compositions is promising due to its simplicity, reliability, and cost-effectiveness. A number of TiO2/SiO2 composite sols were created in Zhao et al. [33]. Tetraethyl orthosilicate and titanium (IV) isopropoxide were employed as precursors in an acidic environment for this aim. The initial hydrolysis stage of tetraethyl orthosilicate increases the stability of binary sols. It is suggested that the top layer of a multilayer coating be composed of a dense SiO_2 film and an ordered mesoporous SiO_2 film. Heat treatment was used to control the hybrid films' refractive index over a broad range. Two types of antireflective coatings with multilayer quarter-half and quarter-half-quarter structures were developed. In the 400-800 nm region, the three-layer coating's optical transmittance is 98.74%, while the two-layer coating's reaches even 99%. The mechanical qualities of both kinds of multilayer coatings are good. Due to the enhanced control of the sol composition, the practical sol-gel method has potential for the production of antireflective coatings.

In the visible region of the spectrum, broadband multilayer ARCs have been developed and manufactured on protective glasses of optoelectronic devices. Along with a silicon photocell, the protective glass is an integral component of an optoelectronic device, in particular, a solar battery [34–36].

In Hassan-Aghaei and Mohebi [35], different types of three-layer mesoporous silicon coatings with graded porosity, produced by the self-assembly method, are compared. The formation of different mesostructure designs in solution occurred due to the change in the concentration of the surfactant. The coatings were applied to the substrate by the method of sequential centrifugation. The effect of the layer arrangement on the light transmission and water absorption was studied. The transparent multilayer coatings produced showed that they have a uniform pore size of about 3 nm and a layer thickness of about 450 nm.

The performance of PV cells decreases with increasing surface temperature, especially in hot weather conditions. Therefore, passive and active cooling systems are used, which increases the cost of their production and application. A technology aimed at creating a composite nanocoating on the surface of a solar panel reduces the cost of maintaining a solar energy system and increases the efficiency of solar panels. In Abbood and Abed [36], the panel's surface was coated with nanocomposite materials like TiO2, ZnO, and CNT. It was discovered that the coating lowers the solar cell's temperature by acting as a heat dissipator. Al₂O₃/SiN/TiO₂/ SiN/SiO₂ multilayer coatings have been shown to reduce temperatures by 5.7 °C in certain results, while other results have shown a temperature reduction of 9.7 °C and an efficiency improvement (+2.3%) with TiO₂ nanoparticles. Such coatings compensate for the drop in output power caused by an increase in the surface temperature of the solar cell and protect it from aging and thermal damage.

As demonstrated above, porous coatings derived from sols exhibit a low refractive index, along with excellent abrasion resistance and endurance. SiO2(TiO2)-based coatings possess high optical transmittance [37–39]. TiO₂/SiO₂ coating is very

promising for protecting PV glass coatings from erosive wear. To improve the erosion resistance, an additional 1 at % Zr-doped coating was applied to the TiO₂/SiO₂ antireflective coatings by magnetron sputtering and annealed at 400 °C. As a result, improved optical (67% reduction in defect level per unit area) and tribological (89% reduction in erosion level) properties were observed compared to the substrate [37].

ARCs usually suffer from poor functional durability when used outdoors. To overcome these drawbacks, efforts have been made to impart additional properties to antireflective coatings, such as selfcleaning and mechanical stability. In Li et al. [38], broadband three-layer interference ARCs were synthesized from SiO₂/TiO₂ and TiO₂ materials. The bottom, middle, and top layers were produced using nanoporous TiO2-SiO2 composite thin films. Transmittance at 500-700 nm was consistently high for the substrates (BK-7 glass) covered with the three-layer films; the average transmittance in this range was 99.4%. The three-layer films showed a 2-degree water contact angle and high superhydrophilic properties. Without exposure to ultraviolet (UV) light, the superhydrophilicity could be sustained for 30 days. Under UV light, these three-layer coatings demonstrated a strong capacity to break down organic materials. The synergistic effect between superhydrophilicity and photocatalysis provides the films with a self-cleaning effect. The abrasion resistance test of the three-layer films showed good strength and adhesion of the films to the substrates.

The use of polymeric materials as a filler in layered nanocomposite antireflective coatings provides high optical transparency in a wide range of wavelengths and superhydrophobicity. A two-layer ARC is shown in Sun et al. [39], with an upper SiO_2 layer modified with hexamethyldisilazane (HMDS) and a lower layer made of SiO_2 — TiO_2 composite nanomaterials. By altering the lower and higher layers' structures, the layers' refractive indices were altered. The optical transmittance in this scenario may be 95.2% and 96.0%, respectively, in the 400–1200 nm and 400–1800 nm ranges. Furthermore, a two-layer coating with superhydrophobic qualities and a hydrophobic angle of 151.4° is produced by altering the top layer with HMDS. The antireflective properties of the two-layer ARC were not substantially altered by tests conducted in environments with high temperatures and humidity levels.

The refractive index of nanocomposite layered coatings can be regulated not only by changing the composition of the layers but also by their porosity without changing the composition. In addition, if the coating has photocatalytic activity, it is capable of self-cleaning from the dirty impurities of the external environment. One of the materials with photocatalytic activity is titanium dioxide. The work by Khan et al. [40] describes a single-component two-layer titanium dioxide coating BT@ARC, consisting of a TiO2 layer based on porous nanorods (n \sim 1.38) and a dense TiO2 layer (n \sim 2.45). The layers were applied by physical vapor deposition. Thermal tests of the coating showed stability of the antireflective ability and improvement of mechanical properties up to 300 °C.

The sol-gel process deposits silicon nanospheres on surfaces, resulting in low refractive index coatings. Introducing hollow structures into silicon nanospheres can result in coatings with an ultra-low refractive index (<1.15). However, it is difficult to realize a simple and large-scale one-step fabrication of hollow silicon nanospheres (HSN) with diameters suitable for transparent optical coatings using current methods. A one-step strategy for the preparation of HSN colloids was proposed in He et al. [41]. Stöber silica nanospheres served as the initial nanoparticles, with their diameters adjusted by varying the

ammonia concentration. Hydrofluoric acid (HF) solutions of varying concentrations were used to etch nanospheres of various sizes, and the structural alterations that occurred prior to and following etching were recorded. The proper coatings for dual-layer broadband antireflection structures were chosen after the etched nanospheres were coated and their refractive indices were determined. The results demonstrated that following HF etching, nanospheres of varying diameters had distinct structural changes. The larger nanospheres were gouged out, while the smaller ones aggregated. This was the first time that HSNs were obtained by a one-step etching method. The refractive index of the etched nanospheres was 1.387–1.057. In this work, a dual-layer broadband ARC with a refractive index of 1.057 and 1.339 as the top and bottom layers, respectively, was designed and fabricated.

Plasmonic nanocomposites, particularly matrix nanocomposites composed of metal-dielectric structures, play a significant role in the development of ARCs. The mechanical and optical properties of such structures are described in Calpe et al. [42], El-Morsy et al. [43], and Khitous et al. [44]. Due to their unique optical characteristics, near-zero epsilon (ENZ) materials have garnered attention lately; yet, their potential is constrained by the material's inherent losses. Periodic media made of alternating layers of ENZ and a dielectric are known as enhanced near-zero epsilon (eENZ) materials. In Calpe et al. [42], a 15-layer thin-film ENZ-dielectric structure was fabricated, in which indium tin oxide (ITO) served as the ENZ material and titanium dioxide as the dielectric. The improved optical transmission of the structure was experimentally demonstrated compared to a bare ENZ film of similar thickness. In addition, a giant polarization-dependent optical response of the material was demonstrated. The physical explanation of these effects is associated by the authors with directed waves, Fabry-Perot resonances, and Ferrell-Berreman plasmons inside the film stack. The experimental implementation carried out in the work opens up prospects for optoelectronic devices using eENZ materials. In El-Morsy et al. [43], ENZ polymer composite nanomaterials incorporating silver nanoparticles (Ag NPs) were prepared via laser ablation, combined with base dielectric films consisting of 50% Polystyrene (PS) and 50% PMMA. The semicrystalline nature of the PS/PMMA matrix was confirmed by two diffraction peaks, attributed to the interaction and complexation between Ag NPs and the PS/PMMA matrix. To illustrate the optical characteristics of the obtained samples, UV-Vis studies were carried out. It was demonstrated that the obtained samples' optical energy gap (Eg) drops from 2.66 to 1.95 eV at indirect transition and from 3.76 to 3.31 eV for direct transition. The alternating current (AC) conductivity spectra of all films were investigated using broadband dielectric spectroscopy. In Khitous et al. [44], a new method for preparing substrates for visible light photocatalytic applications of ENZ composite nanomaterials is presented. It is based on two stages of structure fabrication: sol-gel synthesis of a thin TiO₂ film, followed by spin-coating on the substrate, and thermal drying of a thin gold film to create a dense array of AuNPs. Following methylene blue's N-demethylation reaction as a model reaction, surface-enhanced Raman spectroscopy (SERS) was used to investigate the photocatalytic characteristics of these nanocomposite films. The SERS study aids in assessing the impact of variables like TiO₂ position and thickness (on or under the AuNPs). The study of the photocatalytic properties of AuNP-TiO₂ nanocomposite films is of interest for the creation of self-cleaning antireflective coatings for solar energy. Many optoelectronic devices require coatings that combine optical transparency and electrically conductive properties [45]. One of the main materials for such coatings is TCO of indium tin. However, the homogeneity of the emission characteristics of devices with a high active surface is impacted by the coatings' inadequately low specific resistance. For instance, when utilizing the TCO of indium tin, an organic luminescent display is unable to consistently generate light from the full active region. However, a decrease in the specific resistance of such coatings due to an increase in the density of free charge carriers in the film causes a shift in the plasma frequency to the visible part of the spectrum, which in turn reduces the coating's optical transparency. This problem can be solved by using coatings (electrodes) made of PAAO, as proposed in Nakanishi et al. [46]. High conductivity and transparency over a wide region are provided by PAAO, which also removes the need for rare metals like indium. There are known works in which the optical properties of composite materials based on porous membranes of aluminum oxide and various metals filling the pores are investigated [47, 48]. For composite structures of Cu/Al₂O₃ and Ag/Al₂O₃, the spectral transparency and polarization properties were investigated in Tang et al. [47], where it was experimentally shown that the transparency of the Cu/Al₂O₃ structure is higher than that of the Ag/Al₂O₃ structure in the visible and near-IR spectral regions. In Dhara et al. [48], optically transparent ceramic composite materials were developed based on a porous membrane made of anodic aluminum oxide and gold nanoparticles implanted into the membrane. Gold nanoclusters were grown by implanting 1.8 MeV Au²⁺ into a c-Al₂O₃(0001) substrate, followed by annealing in air at temperatures of 1273 K. After annealing, the samples demonstrated plasmon resonance in the optical region (561-579 nm) with average cluster sizes of 1.72-2.4 nm. For gold in the form of clusters embedded in pores, a shift in the resonant frequency of surface plasmons was observed, depending on the pore size and membrane porosity, both to the short-wavelength region and to the longwavelength region of the optical spectrum.

2.2. Optical spectral properties

Protective glasses, such as low-iron float glass, are commonly used to protect against mechanical damage and improve radiation transmission to receiving elements of optoelectronic devices. However, although these glasses are highly transparent, Fresnel reflection losses of up to 8% occur at the interface due to the difference between the refractive indices of the glass and the surrounding air. To increase the transparency of protective glasses, single-layer and multilayer antireflective coatings are used. In the production of antireflective coatings, it is necessary to meet environmentally friendly conditions. For instance, a novel sol-gel technique for producing thin films from an aqueous medium is introduced in Kócs et al. [49]. From aqueous silicon sols, single-layer antireflective coatings were produced and described. It was found that the thickness of the thin films ranged from 75 to 135 nm with refractive indices from 1.23 to 1.41 and porosity from 7% to 53%. In the visible spectrum, the produced coatings' maximum transmittance ranged from 99.85% to 99.03%. Individual silicon nanoparticles with a limited size distribution (15-20 nm) made up the translucent aqueous sol. Lowering the storage temperature can increase the shelf life of aqueous silicon sols because it influences the kinetic behavior of silicon sols. To prevent particle aggregation in water, the sol was kept in a freezer at -18 °C for three months. For each sample, layers were deposited onto microscope slides at a withdrawal rate of 1.4 mm/s from both newly made (type A) and thawed, frozen (type B) sols. The surfaces of small regions (75 × 26 × 1 mm3) were uniformly coated and showed no signs of surface deterioration. The maximum transmittance of aqueous thin films decreased by only 1.61%: from $99.85 \pm 0.08\%$ at 756 nm to $98.24 \pm 0.19\%$ at 579 nm.

Figure 2
UV-Vis transmission spectra of the silica antireflective coatings compared to the bare microscope glass slide

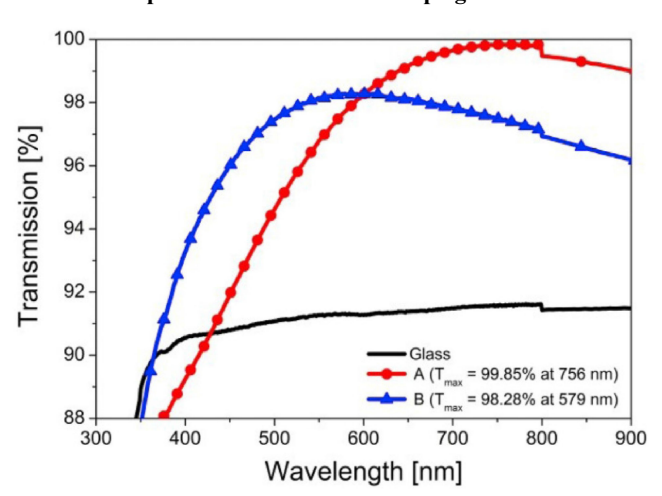
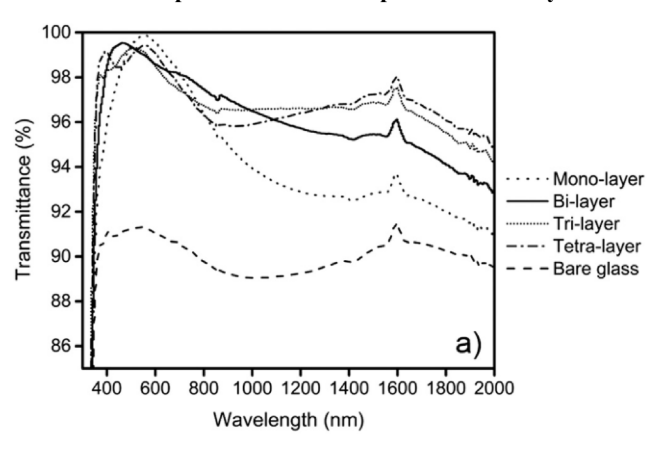


Figure 2 [49] shows thin films of freshly prepared (type A) and thawed (type B) silica sol. The extraction rate was 1.4 mm/s with single-stage heat treatment at 450 °C. From the dependencies shown in Figure 2, it can be concluded that aqueous sols can be stored in a frozen state, since using both fresh and aged sols, it is possible to obtain antireflective coatings with almost the same light transmission.

In order to offer broadband antireflective coatings for glass components in PV applications, multilayer silicon stacks were created in Agustín-Sáenz et al. [50]. Four different kinds of organic and inorganic systems were used to create the porous silicon coverings using a combination of evaporation-induced selfassembly and acid-catalyzed sol-gel techniques. Environmental ellipsometry, porosimetry, and atomic force microscopy were used to study the material structure, while ellipsometry and spectrophotometry were used to assess the optical properties. Both the organic and inorganic phase concentrations were tuned. A broadband antireflective bilayer coating in the wavelength range of 300-2000 nm was fabricated, providing a transmittance enhancement of 7.2% (at solar reference spectral density AM1.5) compared to bare glass. The coatings were deposited on a glass substrate from both sides. For a better understanding of the optical reflection of the four-layer stack, Equations (1)-(5) are given in Agustín-Sáenz et al. [50], which describe the reflections at each interlayer interface. Taking into account the high requirements for the mechanical properties of the outer surface of the four-layer antireflection stack, theoretical calculations were carried out in this work, limiting the value of the void fraction in each layer to 50%. In Equation (6), $d_{\rm n}$ is the layer thickness, λ is the wavelength, and θ_n is the reflection angle of each layer. By varying each layer's thickness and refractive index, the system's overall reflectivity can be reduced. Air is medium 0, the substrate is medium s, and each layer is represented by media 1 through 4 in the reflection equations (Equations (1)–(5)). Equation (6)defines δ_n as the phase angle produced by each layer, n_n as the real part of each material's refractive index, and R_{xy} as the reflection at each interface between x and y media.

$$R_{01} = \frac{n_0 - n_1}{n_0 + n_1} \tag{1}$$

Figure 3
Transmittance spectra of different optimized multilayer stacks



$$R_{12} = \frac{n_1 - n_2}{n_1 + n_2} \exp\left(-2\delta_1\right) \tag{2}$$

$$R_{23} = \frac{n_2 - n_3}{n_2 + n_3} \exp\left(-2(\delta_1 + \delta_2)\right) \tag{3}$$

$$R_{34} = \frac{n_3 - n_4}{n_3 + n_4} \exp\left(-2(\delta_1 + \delta_2 + \delta_3)\right) \tag{4}$$

$$R_{45} = \frac{n_4 - n_5}{n_4 + n_5} \exp(-2(\delta_1 + \delta_2 + \delta_3 + \delta_4))$$
 (5)

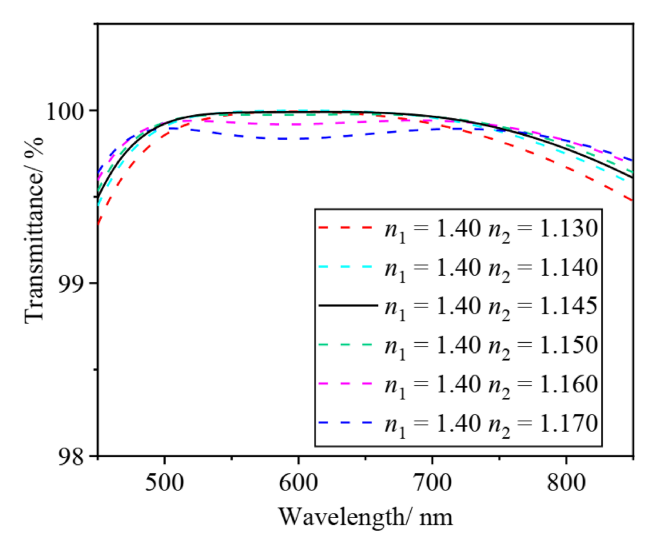
$$\delta_n = \frac{2\pi n_n d_n \cos \theta_n}{\lambda} \tag{6}$$

Using the CODE software, multilayer stack ARCs were developed in the work by minimizing the total reflection in the range of 300–2000 nm. The transmission spectra are shown in Figure 3 [50].

With a void fraction of 11%, 45%, and 77%, the three-layer stack produced a superior transmittance value across the whole working range. However, the outer layer's void percentage was restricted to 50% since high porosity makes layers with poor mechanical qualities more brittle. Spectral differences in the transmission and reflection curves should be noted. The two-layer stack's integrated transmittance values were greater than the three-layer stack's integrated transmittance values were higher than the two-layer stack's in the 980–2000 nm range.

In Liu et al. [51], dual-layer $\lambda/4-\lambda/4$ ARCs exhibiting consistently high transmittance within a specific wavelength range were developed. These coatings were prepared using the sol-gel method, employing acid-base catalyzed SiO2 thin films. The resulting dual-layer antireflective coating had a nearly constant transmittance of 99.8% in the 550-700 nm range. Furthermore, with a variation of less than 1%, the transmittance of this coating was above 99% over a broader range of 450-850 nm. After two weeks of exposure to 50% humidity, the coatings maintained their high transmittance and demonstrated good environmental resilience. The expected optical performance of the dual-layer broadband $\lambda/4-\lambda/4$ coating with constant high transmittance was simulated using TFCalcTM computer software (version 3.5, Software Spectra, Spectra, Portland, OR, USA). For the two-layer ARCs, the central wavelength of each layer was chosen to be 600 nm. Figure 4 [51] displays the simulation results for the two-layer

Figure 4
Simulated transmittance spectra of modeled double-layer coatings



coating with varying refractive indices. Both the top and bottom layers have ideal refractive indices of 1.40 and 1.145, respectively. In the broadband wavelength region of 550–700 nm, the ideal simulated two-layer coating can reach a consistent high transmittance of 99.99%, and in the wider wavelength range of 450–850 nm, it can achieve an average transmittance of 99.75%. In the ideal model, the top and bottom layers are 131 nm and 107 nm thick, respectively.

Figure 5 [51] shows the transmittance spectra of simulated and prepared double-layer broadband ARCs, and the transmittance spectrum of bare glass was also measured.

In Ushakov et al. [52], broadband antireflective coatings were developed for optoelectronic devices of various types – three-layer coatings based on SiO₂/TiO₂/SiO₂, single-layer coatings based on matrix polymer composite nanomaterials made of PMMA with Ag NPs, and membrane nanocomposite coatings based on

Figure 5
Transmission spectra of bare BK7 glass, simulated and experimental double-layer ARCs

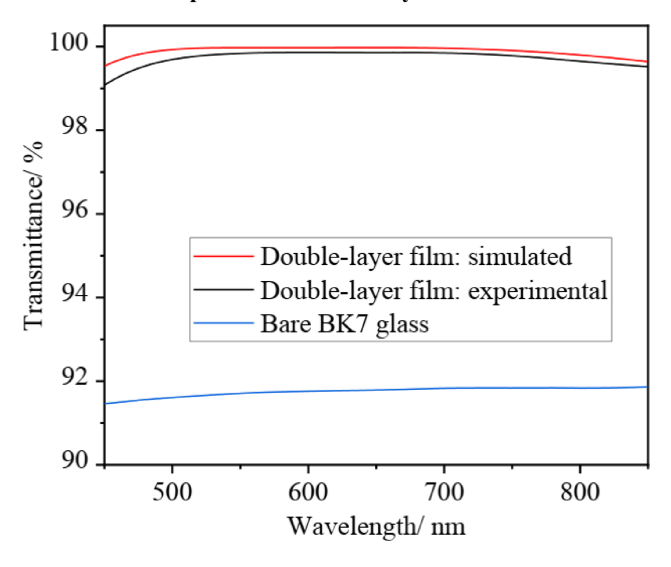


Figure 6
Optical reflection spectra on a glass substrate for a three-layer and a four-layer coating

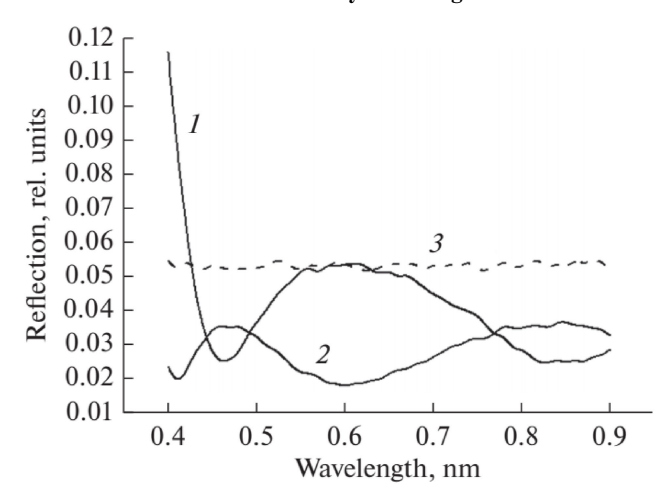


Figure 7
Spectral dependences of the reflectivity of the PMMA coating and composite nanocoating Ag-PMMA on glass

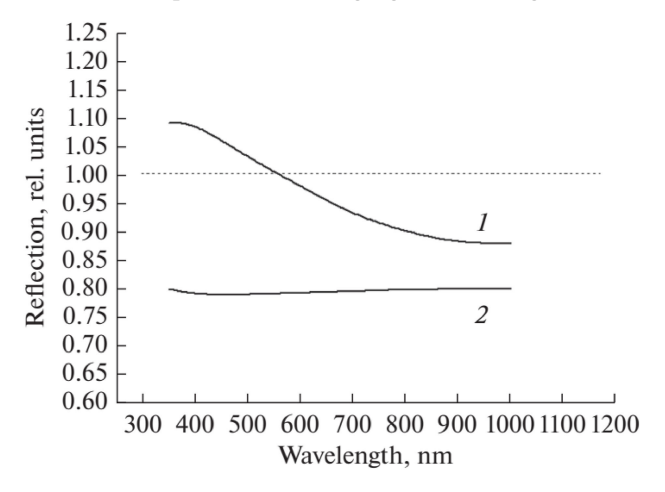


Figure 8
Optical reflectance spectra of free anodic aluminum oxide membrane (1) and with gold film applied (2)

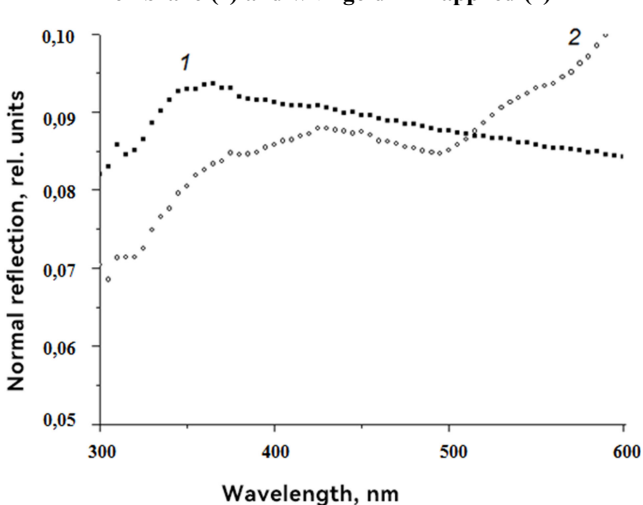


Table 1
Antireflective coatings (ARCs) and conductive transparent elements for optoelectronic devices

Coating material	Functional properties	Transmittance, T (reflectivity, R)	Advantage/drawbacks	Ref
Single layer		Layered dielectric oxides		
coatings				
- SiO ₂ - SiO ₂ @MgF2 hybrid	Sol-gel process. Ecologically safe technology from aqueous silicon sols. Film thickness from 75 to	Transmission 98.1–99.85% (400–800 nm) and 96.6% (300–1500 nm).	High resistance to weather conditions and UV radiation. Broadband antireflective ability.	[49]
-TiO ₂ @SiO ₂ hybrid induced by Zr-oxide doping	135 nm, refractive index from 1.23 to 1.41, porosity from 7 to 53%. Magnetron sputtering SiO ₂ @TiO ₂ , alloying with 1 at.% Zr, annealing at 400 C. High surface homogeneity and adhesion to glass. Easy to clean, anti-fog, weather and UV resistant.		Protection of solar panels from erosive wear, increasing their durability and efficiency (optical and electrical).	[1]
				[37]
Two-layer coatings -The bottom layer is porous SiO ₂ , the top layer is hydrophobic	Sol-gel process. The coating has a hardness class of 6H on a pencil and an adhesion class of 5B on adhesive tape. High self-cleaning ability.	The transmittance of coated glass is 5% higher than that of clean glass. The output power of coated photovoltaic modules is 5.67% higher.	High mechanical properties. Superhydrophobic properties, self-cleaning properties, high durability. Efficient and broadband antireflective ability.	[29]
SiO ₂ . SiO ₂ /SiO ₂ @TiO ₂ hybrid	The top SiO ₂ layer is modified with hexamethyldisilazane (HMDS).	Average transmittance of 96.0 % (400–1800 nm).	Recommended for use in electroluminescent displays.	[39]
- Acid-base catalyzed SiO ₂ thin films	Two-layer $\lambda/4$ - $\lambda/4$ antireflection coatings. Constant high optical transmittance in a given wavelength range.	Transmittance of 99.8% in the 550–700 nm range and exceeded 99% in a broader 450–850 nm range with less than 1% fluctuation.	electroluminescent displays.	[51]
Three-layer				
coatings - Bayberry-like SiO ₂ @TiO ₂	Sol-gel process. Triple-layer graded-index broadband antireflective coatings (TGBA). The high self-cleaning ability of TGBA under environmental exposure, high-cycle ultraviolet (UV) irradiation, and dark storage.	The average transmittance of TGBA-coated glass is 8.93% (380–1800 nm) higher than that of uncoated glass.	Multifunctional coatings can improve the generation efficiency of photovoltaic systems in harsh environments.	[4]
-Mesoporous SiO ₂ films	Three-layer, three-wave broadband ARC. Mesoporous SiO ₂ films with a strong framework and varying porosity provide good abrasion resistance. To increase the surface stability of the antireflective coating layers, they are additionally modified with perfluorodecyltriethoxysilane.	High transmittance of 99.24%, 99.66%, and 99.64% at 351 nm, 527 nm, and 1053 nm, respectively.		[6]
SiO ₂ /Nb ₂ O ₅ / SiO ₂ @TiO ₂ hybrid	Three-layer "quarter-half-quarter" structure with a dense SiO ₂ film as the top layer. The dense top layer provides good abrasion resistance. To improve its hydrophobicity, the surface is modified with hexamethyldisilazane. The refractive index of the Nb ₂ O ₅ film (middle layer) reaches 2.072 (at 550 nm).	The average transmittance reaches 98.41% (400–800 nm).		[23]

Table 1 (Continued)

Coating material				
	Functional properties	Transmittance, T (reflectivity, R)	Advantage/drawbacks	Ref
Single layer nanocomposite		trix polymer nanocomposites		
- (50% PS@50% PMMA)/Ag NPs	Laser ablation. The interaction of silver nanoparticles with the PS/PMMA matrix leads to a change in the intensity of the transmission bands in the UV-visible range.	The band gap (Eg) of the samples decreases from 3.76 to 3.31 eV (direct transition) and from 2.66 to 1.95 eV for indirect transition.	This study may have a significant impact on optoelectronic devices and energy storage applications. No optical transmission data are provided.	[43]
PMMA/Ag NPs	The synthesis of silver nanoparticles in a polymethyl methacrylate matrix is based on the reduction of the ammonia complex in a polymer solution in 1,2-dichloroethane with slight heating of the reaction mixture (T = 70 ° C). The coatings were applied to glass substrates by a drop method from the liquid phase of Ag–PMMA powder and mechanically distributed uniformly over the surface of the substrate using a squeegee. The PMMA films with a thickness of 5–50 μm with a silver concentration of 0–15 wt.%, applied to a glass substrate, were studied.	Only films with a mass concentration of silver nanoparticles of 1–3 wt.% had antireflective ability and high transmittance. Optical reflection in the range of 300–1000 nm of samples with an applied composite film was 20% lower than for glass with a clean surface.	Optical characteristics weakly depend on the coating thickness. Recommended coating thickness range from 10 µm to 100 µm. Broadband antireflective ability. High requirements for the mass concentration of silver nanoparticles.	[52]
M k	Trans	sparent conducting oxide films		
Membranes - TCO films	Vacuum magnetron sputtering. Electrochemical anodizing oxidation. The current goal is to deposit p-type TCO films. Such p- type materials include thin films of ZnO:Mg, ZnO:N, ZnO:In, NiO, NiO:Li, CuAlO ₂ , Cu ₂ SrO ₂ , and CuGaO ₂ . P-type TCO materials are needed for the development of solid-state lasers.	Average optical transmittance > 80% (450–1100 nm). Minimum resistivity 0.001 Ohm cm.	Combination of electrical conductivity and optical transparency. Shortage and high cost of In, instability at temperatures above 200 °C. Search for alternatives that are more stable in acidic, alkaline, oxidizing, reducing and elevated temperatures. It is necessary to develop methods for film deposition over large areas.	[45]
- PAAO/Au	Synthesis of PAAO/Au membrane. Electrochemical anodic oxidation of aluminum. Vacuum deposition of gold metal film. The membranes had the following parameters: average pore length – 11 μm; average pore diameter – 65 nm; interpore distance – 105 nm; porosity – 35%. The pores were arranged hexagonally. The gold film had a mesoporous structure with grain sizes within 25–30 nm and partly covered the inner walls of pores.	Spectral optical characteristics were studied in the wavelength range of 200–900 nm. It was found that the gold film changes the spectral characteristics of the composite membrane only at wavelengths above 500 nm. The transmission spectrum has a maximum at 500 nm, which is due to the onset of growth in light absorption by the gold film at longer wavelengths. The presence of a thin gold film ensures the surface conductivity of the membrane at a level of 3.4 × 10 Ohm–1 m–1, maintaining optical transparency within	Recommended as transparent conductive electrodes in optoelectronic devices with a large active area of the light transmitter/receiver. Insufficient broadband optical transparency.	[53]
		10–20%.		

Table 1	
(Continued))

Coating material	Functional properties	Transmittance, T (reflectivity, R)	Advantage/drawbacks	Ref
	substrate. The novel transparent multilayer conductive coatings have a honeycomb-shaped metaglass structure. Using visible-transparent silver-based conductive coatings on each side of the glass substrate modifies the electromagnetic properties of the glass substrate.	optical transmittances of 83% and 78% at frequencies and wavelengths of 28 GHz and 550 nm, respectively.	including automotive radar systems. An alternative to standard indium tin oxide (ITO) transparent material. This research opens the way to the development of new visible-transparent metamaterials and artificial dielectrics.	

Au/PAAO. On the glass substrate, the three-layer coatings were as follows: the bottom layer was 84 nm thick and had a SiO₂/TiO₂ refractive index of 1.78; the middle layer was 134 nm thick and had a refractive index of 2.24; and the top layer was comparable to the bottom layer (refer to Figure 6 [52], curve 1). The four-layer glass coatings produced the best results. The structure of the four-layer coatings that were created for the glass substrate was as follows: (1) the SiO₂–TiO₂ layer, which is 84 nm thick and has a refractive index of 1.78; (2) the TiO₂ layer, which is 67 nm thick and has a refractive index of 2.24; (3) the layer that resembles layer 1; and (4) the SiO₂ layer, which is 103 nm thick and has a refractive index of 1.45 (Figure 6, curve 2). For comparison, the spectrum reflection of light off a glass substrate surface (curve 3) is displayed in Figure 6.

In Ushakov et al. [52], antireflective coatings were also made from polymer composite nanomaterials based on PMMA with Ag NPs embedded in its volume. The PMMA films had a thickness of 5–50 μ m, and the concentration of Ag NPs was from 0 to 15 wt.%. Figure 7 [52] shows the experimental spectral dependences of the reflectivity of the PMMA polymer coating (curve 1) and the Ag@PMMA composite coating (curve 2) of the same thickness of 10 μ m. The value of the reflectivity of a pure glass substrate was taken as a unit. The best results in optical reflection were shown by polymer coatings with a mass concentration of silver of 1–3%. Such coatings provide 20% lower reflection losses compared to a glass substrate.

Samples of porous aluminum oxide membranes with an open surface (curve 1) and with a gold layer applied to the reverse side of the membrane (curve 2) exhibit optical spectrum dependences of light reflection, as illustrated in Figure 8 [53]. In the range from 350 nm to 520 nm, the membrane with the gold film has a light reflection comparable to that of a glass substrate (about 8%). An increase in optical reflection to 10% is detected only after 520 nm. The specific conductivity of a gold film 100 nm thick was 3.4×10^6 S/m.

Table 1 presents the main types of antireflective coatings and electrically conductive transparent elements that have found and can find wide application in various optoelectronic devices.

3. Conclusion

The review presents literature data on the development of single-layer and multilayer ARCs based on metamaterials from porous oxide and polymer composite nanomaterials. Particular attention is paid to porous film dielectric materials such as silicon dioxide, titanium dioxide, ceramic membranes made of porous anodic aluminum oxide, and polymer composite nanomaterials based on PMMA with Ag NPs. Layered coatings made of porous

oxide composite materials are capable of providing high adhesion to glass substrates, self-cleaning of the surface from external contaminants, and, on average, increasing the light transmission of protective glass in the optical wavelength range from 300 to 1000 nm. In our opinion, the most optimal structure for ARCs should be considered a two-layer structure of porous SiO2 (top layer) and a hybrid bottom layer (SiO₂/TiO₂) with a controlled composition of the layers. The article also presents the results of studying the optical transmission (reflection) spectra of the synthesized singlelayer thick-film (5-50 µm) polymer composite Ag/PMMA nanostructures. The optimal option for obtaining a possible antireflection effect in such structures is the creation of coatings with a silver concentration of 1-3 wt.%. Metaglasses (a glass plate with silver-metallized surfaces) and membranes made of porous anodic aluminum oxide with a deposited thin gold film are considered promising electrically conductive and optically transparent elements. In our opinion, the priority areas of research in the field of new metamaterials with antireflective properties in layered structures should be considered the search for materials for the upper layer with a low refractive index, capable of selfcleaning from external contaminants, and the lower hybrid layer with good adhesion to the glass surface. As an alternative to the standard electrically conductive optically transparent material based on ITO, it is necessary to develop new electrically conductive metamaterials and artificial dielectrics that are transparent for the visible and near-IR spectral range.

Ethical Statement

This study does not contain any studies with human or animal subjects performed by any of the authors.

Conflicts of Interest

The authors declare that they have no conflicts of interest to this work.

Data Availability Statement

Data sharing is not applicable to this article as no new data were created or analyzed in this study.

Author Contribution Statement

Nickolay M. Ushakov: Writing – original draft, Writing – review & editing, Visualization, Supervision, Project administration. I. D. Kosobudskiy: Validation, Formal analysis. M. Yu. Vasilkov: Investigation, Resources.

References

- [1] Joshi, D. N., Atchuta, S. R., Lokeswara Reddy, Y., Naveen Kumar, A., & Sakthivel, S. (2019). Super-hydrophilic broadband anti-reflective coating with high weather stability for solar and optical applications. *Solar Energy Materials* and Solar Cells, 200, 110023. https://doi.org/10.1016/j. solmat.2019.110023
- [2] Suzuki, R. (2023). Fabrication of a porous SiO₂ thin film with an ultralow refractive index for anti-reflective coatings. *Journal* of Sol-Gel Science and Technology, 106(3), 860–868. https:// doi.org/10.1007/s10971-023-06108-8
- [3] Huang, J. Y., Wang, Y., Tao Fei, G., Xu, S. H., Zeng, Z., & Wang, B. (2023). TiO₂/ZnO double-layer broadband antireflective and down-shifting coatings for solar applications. *Ceramics International*, 49(7), 11091–11100. https://doi.org/10.1016/j.ceramint.2022.11.305
- [4] Wu, J., Tu, J., Hu, K., Xiao, X., Li, L., Yu, S., ..., & Yang, Y. (2022). Sol-gel-derived bayberry-like SiO₂@TiO₂ multifunctional antireflective coatings for enhancing photovoltaic power generation. *Colloids and Surfaces A: Physicochemical and Engineering Aspects*, 654, 130173. https://doi.org/10.1016/j.colsurfa.2022.130173
- [5] Keshavarz Hedayati, M., Abdelaziz, M., Etrich, C., Homaeigohar, S., Rockstuhl, C., & Elbahri, M. (2016). Broadband anti-reflective coating based on plasmonic nanocomposite. *Materials*, 9(8), 636. https://doi.org/10.3390/ma9080636
- [6] Qu, J., Jia, H., Wang, W., Wang, Y., & Zhu, S. (2023). Design and implementation of three-layer mesoporous silica coating for tri-wavelength broadband antireflection by block copolymer assisted sol–gel method. *Silicon*, 15(11), 4959–4966. https://doi.org/10.1007/s12633-023-02411-9
- [7] Wang, Z., Yang, P., Qi, G., Zhang, Z. M., & Cheng, P. (2020). An experimental study of a nearly perfect absorber made from a natural hyperbolic material for harvesting solar energy. *Journal* of *Applied Physics*, 127(23), 233102. https://doi.org/10.1063/5. 0005700
- [8] Zhao, J., Zhang, C., Cheng, Q., Yang, J., & Cui, T. J. (2018). An optically transparent metasurface for broadband microwave antireflection. *Applied Physics Letters*, 112(7), 073504. https://doi.org/10.1063/1.5018017
- [9] Santonocito, A., Patrizi, B., & Toci, G. (2023). Recent advances in tunable metasurfaces and their application in optics. *Nanomaterials*, 13(10), 1633. https://doi.org/10.3390/ nano13101633
- [10] Sugimoto, H., & Fujii, M. (2021). Magnetic Purcell enhancement by magnetic quadrupole resonance of dielectric nanosphere antenna. ACS Photonics, 8(6), 1794–1800. https://doi.org/10.1021/acsphotonics.1c00375
- [11] Wang, M., Krasnok, A., Lepeshov, S., Hu, G., Jiang, T., Fang, J., ..., & Zheng, Y. (2020). Suppressing material loss in the visible and near-infrared range for functional nanophotonics using bandgap engineering. *Nature Communications*, 11(1), 5055. https://doi.org/10.1038/s41467-020-18793-y
- [12] Yao, R., Sugimoto, H., Feng, T., Fujii, M., Liu, S., Li, X., ..., & Li, G.-C. (2024). Achieving ideal magnetic light emission with electric-type emitters. *Nano Letters*, 24(42), 13315–13323. https://doi.org/10.1021/acs.nanolett.4c03760
- [13] Jia, Y., Tian, Z., Liu, Q., Mou, Z., Mo, Z., Tian, Y., ..., & Gu, Y. (2024). Cascade enhancement and efficient collection of single photon emission under topological protection. *Nano Letters*, 24(39), 12277–12284. https://doi.org/10.1021/acs.nanolett.4c03588

- [14] Adachi, M., Sugimoto, H., Morita, K., Maruyama, T., & Fujii, M. (2024). Scattering/fluorescence dual-mode imaging in MnO₂-coated silicon nanospheres for cancer cell detection. *ACS Applied Materials & Interfaces*, 16(26), 33963–33970. https://doi.org/10.1021/acsami.4c05152
- [15] Jia, W., Liu, M., Lu, Y., Feng, X., Wang, Q., Zhang, X., ..., & Han, J. (2021). Broadband terahertz wave generation from an epsilon-near-zero material. *Light: Science & Applications*, 10(1), 11. https://doi.org/10.1038/s41377-020-00452-y
- [16] Serebryannikov, A. E., & Ozbay, E. (2024). Exploring localized ENZ resonances and their role in superscattering, wideband invisibility, and tunable scattering. *Scientific Reports*, 14(1), 1580. https://doi.org/10.1038/s41598-024-51503-y
- [17] Chen, J., Liu, X., Wang, P., Xiao, C., Chen, S., & Zhou, H. (2024). Epsilon-near-zero material-based bi-layer metamaterials for selective mid-infrared radiation. *Nanotechnology*, 35(5), 055302. https://doi.org/10.1088/1361-6528/ad074f
- [18] Kohn, R. V., & Venkatraman, R. (2024). Complex analytic dependence on the dielectric permittivity in ENZ materials: The photonic doping example. *Communications on Pure and Applied Mathematics*, 77(2), 1278–1301. https://doi.org/10.1002/cpa.22138
- [19] Ikeda, K., Liu, T., Ota, Y., Kobayashi, N., & Iwamoto, S. (2024). Enhanced magneto-optical effects in epsilon-nearzero indium tin oxide at telecommunication wavelengths. *Advanced Optical Materials*, 12(2), 2301320. https://doi.org/ 10.1002/adom.202301320
- [20] Zheng, H., Zheng, Y., Ouyang, M., Fan, H., Dai, Q., Liu, H., & Wu, L. (2024). Electromagnetically induced transparency enabled by quasi-bound states in the continuum modulated by epsilon-near-zero materials. *Optics Express*, *32*(5), 7318–7331. https://doi.org/10.1364/OE.517111
- [21] Singh, H., Kumar, S., & Sharma, P. K. (2024). Investigation of epsilon near zero modes from Drude-Lorentz optical modelling of reflectance spectrum in plasmonic CuS nanostructured films. *AIP Conference Proceedings*, 2995(1), 020072. https://doi.org/ 10.1063/5.0178049
- [22] Wu, J., Tu, J., Li, L., Xiao, X., Hu, K., Yu, S., ..., & Wu, H. (2022). Gradient refractive index-based broadband antireflective coatings and application in silicon solar modules. Surfaces and Interfaces, 30, 101918. https://doi.org/10.1016/j.surfin.2022.101918
- [23] Xu, S., Jia, H., Wang, C., Zhao, W., Wang, Y., Yang, C., ..., & Wang, Q. (2020). Low-temperature preparation of SiO₂/Nb₂O₅/TiO₂–SiO₂ broadband antireflective coating for the visible via acid-catalyzed sol–gel method. *Coatings*, 10(8), 737. https://doi.org/10.3390/coatings10080737
- [24] He, T., Qian, Z., Wang, Q., Zhang, Y., Wang, H., Zhang, J., & Xu, Y. (2023). One step coating anti-reflective SiO₂ film for silicon solar cells applications by atmospheric pressure plasma jet. *Materials Letters*, 350, 134915. https://doi.org/10.1016/j.matlet.2023.134915
- [25] Eessaa, A. K., & El-Shamy, A. M. (2023). Review on fabrication, characterization, and applications of porous anodic aluminum oxide films with tunable pore sizes for emerging technologies. *Microelectronic Engineering*, 279, 112061. https://doi.org/10.1016/j.mee.2023.112061
- [26] Shang, G., Bi, D., Gorelik, V. S., Fei, G., & Zhang, L. (2023). Anodic alumina photonic crystals: Structure engineering, optical properties and prospective applications. *Materials Today Communications*, 34, 105052. https://doi.org/10.1016/j.mtcomm.2022.105052

- [27] Danks, A. E., Hall, S. R., & Schnepp, Z. (2016). The evolution of 'sol-gel' chemistry as a technique for materials synthesis. *Materials Horizons*, 3(2), 91–112. https://doi.org/10.1039/C5MH00260E
- [28] Mikolei, J. J., Richter, D., Pardehkhorram, R., Helbrecht, C., Schabel, S., Meckel, T., ..., & Andrieu-Brunsen, A. (2023). Nanoscale pores introduced into paper *via* mesoporous silica coatings using sol–gel chemistry. *Nanoscale*, 15(20), 9094–9105. https://doi.org/10.1039/D3NR01247F
- [29] Wang, P., Yan, X., Zeng, J., Luo, C., & Wang, C. (2022). Antireflective superhydrophobic coatings with excellent durable and self-cleaning properties for solar cells. *Applied Surface Science*, 602, 154408.https://doi.org/10.1016/j.apsusc.2022. 154408
- [30] Fehlen, P., Guise, J., Thomas, G., Gonzalez-Posada, F., Loren, P., Cerutti, L., ..., & Taliercio, T. (2024). Engineering the infrared optical response of plasmonic structures with ε-near-zero III-V semiconductors. *Advanced Optical Materials*, 12(4), 2301656. https://doi.org/10.1002/adom.202301656
- [31] Ma, Y., Wang, N., Liu, Q., Tian, Y., Tian, Z., & Gu, Y. (2024). Entangled dark state mediated by a dielectric cavity within epsilon-near-zero materials. *Nanotechnology*, 35(23), 235002. https://doi.org/10.1088/1361-6528/ad2e4b
- [32] Walshe, J., Girtan, M., McCormack, S., Doran, J., & Amarandei, G. (2021). Exploring the development of nanocomposite encapsulation solutions for enhancing the efficiency of PV systems using optical modelling. *Optical Materials*, 111, 110654. https://doi.org/10.1016/j.optmat.2020.110654
- [33] Zhao, W., Jia, H., Qu, J., Yang, C., Wang, Y., Zhu, J., ..., & Liu, G. (2023). Sol-gel synthesis of TiO₂-SiO₂ hybrid films with tunable refractive index for broadband antireflective coatings covering the visible range. *Journal of Sol-Gel Science and Technology*, 107(1), 105–121. https://doi.org/10.1007/s10971-021-05719-3
- [34] Hou, G., García, I., & Rey-Stolle, I. (2021). High-low refractive index stacks for broadband antireflection coatings for multijunction solar cells. *Solar Energy*, 217, 29–39. https://doi.org/10.1016/j.solener.2021.01.060
- [35] Hassan-Aghaei, F., & Mohebi, M. M. (2023). Synthesis and characterization of novel multi-layer silica thin films with tailored mesostructure as anti-reflective coatings. *Optical Materials*, 135, 113246. https://doi.org/10.1016/j.optmat.2022.113246
- [36] Abbood, A. M., & Abed, Q. A. (2023). Using the nano-composite coating technology to improve PV solar cell performance: A review. *AIP Conference Proceedings*, 2776(1), 090001. https://doi.org/10.1063/5.0136542
- [37] Zambrano-Mera, D. F., Espinoza-González, R., Rosenkranz, A., Harvey, T. J., Polcar, T., Valenzuela, P., & Gacitúa, W. (2023). Enhanced erosion resistance of anti-reflective TiO₂/SiO₂ coatings induced by Zr-oxide doping. Solar Energy Materials and Solar Cells, 250, 112079. https://doi.org/10.1016/j.solmat.2022.112079
- [38] Li, Y., Yang, K., Xia, B., Yang, B., Yan, L., He, M., ..., & Jiang, B. (2017). Preparation of mechanically stable triple-layer interference broadband antireflective coatings with self-cleaning property by sol–gel technique. *RSC Advances*, 7(24), 14660–14668. https://doi.org/10.1039/C7RA00844A
- [39] Sun, X., Hu, K., Tu, J., & Chen, K. (2021). Design and preparation of superhydrophobic, broadband and double-layer antireflective coatings. *Surfaces and Interfaces*, 24, 101135. https://doi.org/10.1016/j.surfin.2021.101135
- [40] Khan, S. B., Zhang, Z., & Lee, S. L. (2020). Single component: Bilayer TiO₂ as a durable antireflective coating. *Journal of*

- *Alloys and Compounds*, *834*, 155137. https://doi.org/10.1016/j.jallcom.2020.155137
- [41] He, M., Wang, P., Xiao, P., Jia, X., Luo, J., & Jiang, B. (2023). Hollow silica nanospheres synthesized by one-step etching method to construct optical coatings with controllable ultralow refractive index. *Colloids and Surfaces A: Physicochemical and Engineering Aspects*, 670, 131433. https://doi.org/10.1016/j.colsurfa.2023.131433
- [42] Calpe, R., Karvinen, P., Pääkkönen, P., Ornigotti, M., Caglayan, H., Turunen, J., ..., & Koivurova, M. (2024). Observation of enhanced epsilon-near-zero effects in resonant stratified media. *Applied Physics Letters*, 124(9), 091701. https://doi.org/10.1063/5.0178857
- [43] El-Morsy, M. A., Awwad, N. S., Ibrahium, H. A., Bajaber, M. A., Farea, M. O., & Menazea, A. A. (2023). Optical and electrical conductivity improvement of polystyrene/polymethyl methacrylate blend embedded by silver nanoparticles for electrical devices. *Journal of Materials Science: Materials in Electronics*, 34(14), 1162. https://doi.org/10.1007/s10854-023-10549-w
- [44] Khitous, A., Noel, L., Molinaro, C., Vidal, L., Grée, S., & Soppera, O. (2024). Sol-gel TiO₂ thin film on Au nanoparticles for heterogeneous plasmonic photocatalysis. ACS Applied Materials & Interfaces, 16(8), 10856–10866. https://doi.org/10.1021/acsami.3c15866
- [45] Afre, R. A., Sharma, N., Sharon, M., & Sharon, M. (2018). Transparent conducting oxide films for various applications: A review. *Reviews on Advanced Materials Science*, 53(1), 79–89. https://doi.org/10.1515/rams-2018-0006
- [46] Nakanishi, T., Tsutsumi, E., Masunaga, K., Fujimoto, A., & Asakawa, K. (2011). Transparent aluminum nanomesh electrode fabricated by nanopatterning using self-assembled nanoparticles. *Applied Physics Express*, 4(2), 025201. https://doi.org/10.1143/APEX.4.025201
- [47] Tang, H., Wu, F., Wei, Y., & Li, Q. (2005). Comparison of optical properties of Cu-Al₂O₃ and Ag-Al₂O₃ nano-array composite structure. *Chinese Optics Letters*, 3(12), 722–724.
- [48] Dhara, S., Sundaravel, B., Ravindran, T. R., Nair, K. G. M., David, C., Panigrahi, B. K., ..., & Chen, K. H. (2004). 'Spillout' effect in gold nanoclusters embedded in c-Al₂O₃(0001) matrix. *Chemical Physics Letters*, *399*(4–6), 354–358. https://doi.org/10.1016/j.cplett.2004.10.011
- [49] Kócs, L., Jilavi, M. H., Koch, M., & de Oliveira, P. W. (2020). An environmentally friendly approach to produce single-layer anti-reflective coatings on large surfaces using wet chemical method. *Ceramics International*, 46(16), 25865–25872. https://doi.org/10.1016/j.ceramint.2020.07.069
- [50] Agustín-Sáenz, C., Sánchez-García, J. Á., Machado, M., Brizuela, M., Zubillaga, O., & Tercjak, A. (2018). Broadband antireflective coating stack based on mesoporous silica by acid-catalyzed sol-gel method for concentrated photovoltaic application. Solar Energy Materials and Solar Cells, 186, 154–164. https://doi.org/10.1016/j.solmat.2018.06.040
- [51] Liu, H., Wang, P., Fan, Q., Luo, J., Xiao, P., & Jiang, B. (2022). λ/4–λ/4 double-layer broadband antireflective coatings with constant high transmittance. *Coatings*, 12(4), 435. https://doi. org/10.3390/coatings12040435
- [52] Ushakov, N. M., Kosobudskii, I. D., Vasilkov, M. Y., & Mikhailov, I. N. (2022). Optical antireflection matrix and porous metamaterials for optoelectronic devices. *Journal of Communications Technology and Electronics*, 67(10), 1271–1276. https://doi.org/10.1134/S10642269221 00151

- [53] Ushakov, N. M., Vasilkov, M. Y., & Fedorov, F. S. (2017). The influence of a thin gold film on the optical spectral characteristics of a porous anodic aluminum-oxide membrane. *Technical Physics Letters*, 43(7), 648–651. https://doi.org/10.1134/S1063785017070276
- [54] Safari, M., He, Y., Kim, M., Kherani, N. P., & Eleftheriades, G. V. (2020). Optically and radio frequency (Rf) transparent

meta-glass. *Nanophotonics*, *9*(12), 3889–3898. https://doi.org/10.1515/nanoph-2020-0056

How to Cite: Ushakov, N. M., Kosobudskiy, I. D., & Vasilkov, M. Y. (2025). Optical Antireflective Layered and Nanoporous Metamaterials for Optoelectronic Devices. *Journal of Optics and Photonics Research*. https://doi.org/10.47852/bonviewJOPR52025894